Microsecond Protein Dynamics Measured by $^{13}C^{\alpha}$ Rotating-Frame Spin Relaxation

Patrik Lundström and Mikael Akke*[a]

NMR spin relaxation in the rotating frame ($R_{1\rho}$) is a unique method for atomic-resolution characterization of conformational (chemical) exchange processes occurring on the microsecond timescale. We present a rotating-frame $^{13}C^{\alpha}$ relaxation dispersion experiment for measuring conformational dynamics in uniformly ^{13}C-labeled proteins. The experiment was validated by using the E140Q mutant of the C-terminal fragment of calmodulin, which exhibits significant conformational exchange between two major conformations, as gauged from previous ^{15}N and ^{1}H relaxation studies. Consistent with previous work, the present $^{13}C^{\alpha}$ $R_{1\rho}$ experiment detects conformational-exchange dynamics throughout the protein. The average correlation time of $\langle\tau_{ex}\rangle = 25 \pm 8\ \mu s$ is in excellent agreement with those determined previously from ^{1}H and ^{15}N $R_{1\rho}$ relaxation data: $\langle\tau_{ex}\rangle = 19 \pm 7$ and $21 \pm 3\ \mu s$, respectively. The extracted chemical-shift differences between the exchanging states reveal significant fluctuations in dihedral angles within single regions of Ramachandran φ–ψ space, that were not identified from the ^{1}H and ^{15}N relaxation data. The present results underscore the advantage of using several types of nuclei to probe exchange dynamics in biomolecules.

Introduction

The intramolecular dynamics of biomolecules are intimately connected to their biological function. In addition to the time-averaged structure, the conformational dynamics around the mean atomic positions and transitions between distinct substates are critically important for a complete description of biomolecular function. Dynamics on different timescales have different biological significance. For example, motions on the picosecond-to-nanosecond timescale can make significant entropic contributions to the free energy,[1–3] while slower events in the microsecond-to-millisecond range are important for processes such as enzymatic catalysis[4,5] or ligand binding and allosteric regulation.[6–9] NMR spin-relaxation experiments are uniquely suited for the characterization of intramolecular dynamics of small-to-medium-sized biomolecules in solution, since they provides a means to monitor dynamics at virtually every atomic position in the molecule. Slow dynamics can be characterized by Carr–Purcell–Meiboom–Gill (CPMG) or rotating-frame spin-lock ($R_{1\rho}$) relaxation experiments.[10] In both classes of experiments, conformational (chemical) exchange is manifested as dispersion in the transverse-relaxation rate as a function of the applied radio frequency (RF) effective field strength.[10] Typically, $R_{1\rho}$ is the method of choice for studying exchange processes on timescales in the order of 100 μs or shorter, which are normally not accessible by CPMG experiments due to limits on the achievable effective fields. Exchange rates, populations, and the chemical-shift difference between the exchanging states can be extracted by fitting model functions to the relaxation dispersion profile.[9,10] In cases in which the exchange rate is fast on the chemical-shift timescale, the extracted parameters comprise the exchange rate and the product of the populations and chemical-shift difference (see Experimental Section for details). In principle, the chemical-shift difference can be interpreted in structural terms, although this is rarely straightforward unless suitable reference states exist.[6,11–15] Since the chemical shifts of different types of nuclei depend on different conformational parameters,[16,17] a more complete picture of the underlying motions can be obtained by monitoring relaxation dispersions of multiple nuclei (e.g., ^{1}H, ^{13}C, ^{15}N).[18–20] The majority of reports published to date have utilized ^{15}N to probe microsecond-to-millisecond motions of the protein backbone, while a limited number of studies have been performed on the amide ^{1}H,[18,20,21] carbonyl ^{13}C,[22,23] and methyl ^{13}C spins.[24] The ^{15}N chemical shift is an intricate function of several conformational parameters, including local backbone $\psi(i-1)$, $\varphi(i)$, and $\psi(i)$ dihedral angles, side chain $\chi_1(i-1)$ and $\chi_1(i)$ dihedral angles, and hydrogen bonding.[17,25] Likewise, the amide ^{1}H chemical shift is governed by the combined effects of local secondary structure, hydrogen bonding, and long-range ring-current interactions.[16] In contrast, the $^{13}C'$ and $^{13}C^{\alpha}$ chemical shifts depend primarily on the local $\varphi(i)$ and $\psi(i)$ angles.[17] The average root-mean-square (rms) deviation from the mean of the $^{13}C^{\alpha}$ chemical shift varies between 1.34 ppm (for Gly) and 3.44 ppm (for Cys), as gauged from the BioMagResBank (www.bmrb.wisc.edu). Converted to frequency units, this is comparable to the shift differences observed for ^{15}N; this implies that dihedral-angle fluctuations on the μs–ms timescale should be amenable to study by $^{13}C^{\alpha}$ relaxation dispersion experiments. Given the clear dependence of the $^{13}C^{\alpha}$ chemical shift on the (φ, ψ) dihedral angles, $^{13}C^{\alpha}$ $R_{1\rho}$ experiments are particularly powerful for studying fast folding events, such as helix formation, as reported previously for samples specifically labeled with ^{13}C in the α-position.[26] Pioneering work by Yamazaki et al. has shown that accurate measure-

[a] *P. Lundström, Prof. M. Akke*
Department of Biophysical Chemistry, Lund University
P.O.Box 124, 22100 Lund (Sweden)
Fax: (+46) 46-222-4543
E-mail: mikael.akke@bpc.lu.se

 DOI: 10.1002/cbic.200500086

ment of $R_{1\rho}$ can also be attained for uniformly ^{13}C-labeled proteins.[27] However, to the best of our knowledge, the full potential of $^{13}C^{\alpha}$ $R_{1\rho}$ dispersion experiments for characterizing conformational exchange in uniformly ^{13}C-labeled proteins has not been demonstrated previously.

In this paper, we present an approach for measuring $^{13}C^{\alpha}$ on- and off-resonance $R_{1\rho}$ rates that yield exchange rates and estimated chemical-shift differences. The pulse sequence was validated by using the E140Q mutant of the C-terminal fragment (Tr2C; $M_r = 8$ kDa) of calmodulin (CaM) and benchmarked against previous results obtained from ^{15}N and ^{1}H $R_{1\rho}$ experiments.[11,20] The calcium-saturated state of E140Q–Tr2C exchanges between conformations that resemble the closed (apo) and open (calcium-saturated) states of the wild-type domain (wt-Tr2C), as gauged from the $^{1}H/^{15}N$ chemical shifts and pattern of NOESY cross peaks.[11,28,29] The conformational changes between apo and calcium-saturated wt-Tr2C include extensive repacking of the hydrophobic core, changes in side-chain dihedral angles, reorientations of the α-helices, and exposure of a hydrophobic surface, but no significant change in secondary structure.[30–33] This conformational switch is essential for target recognition of a large number of proteins by CaM.[34,35] Previous ^{15}N relaxation dispersion experiments yielded an exchange correlation time of $\tau_{ex} = 21$ μs at 28 °C, and further suggested that the two dominating populations are approximately equal.[11] The exchange correlation time matches approximately with the inverse of the calcium dissociation rate from wild-type CaM; this suggests that ion release is gated by conformational changes in the protein.[11] In addition to providing insights into the molecular basis for the biological function of calmodulin, studies on E140Q–Tr2C also provide valuable biophysical data on large-scale conformational transitions between different native states, and serve as a test bed for developing relaxation dispersion methods that target microsecond timescale dynamics.

Results and Discussion

We designed an experiment for measuring on- and off-resonance $R_{1\rho}$ decay rates of $^{13}C^{\alpha}$ spin magnetizations in uniformly ^{13}C-labeled proteins. A representative $^{1}H,^{13}C$ correlation spectrum of E140Q–Tr2C, obtained by using a relaxation delay of $t_{SL} = 40$ ms, is shown in Figure 1. As observed, the spectral resolution in the $^{13}C^{\alpha}$ region is satisfactory for a protein of this size. We analyzed 50 out of the 73 residues of E140Q–Tr2C. Residues that were not analyzed suffered from either extensive line broadening (F89, I125, D133, Y138), severe spectral overlap with other residues (R106/E139, M124/R126, Q140/M144, E82/E120/E123), or with residual intensity from the solvent (D80, N97, L116, N137). In addition, all five glycines (G96, G98, G113, G132, G134) were excluded from the analysis, because optimal magnetization transfer cannot be achieved simultaneously for spin systems with one or two attached protons.[36]

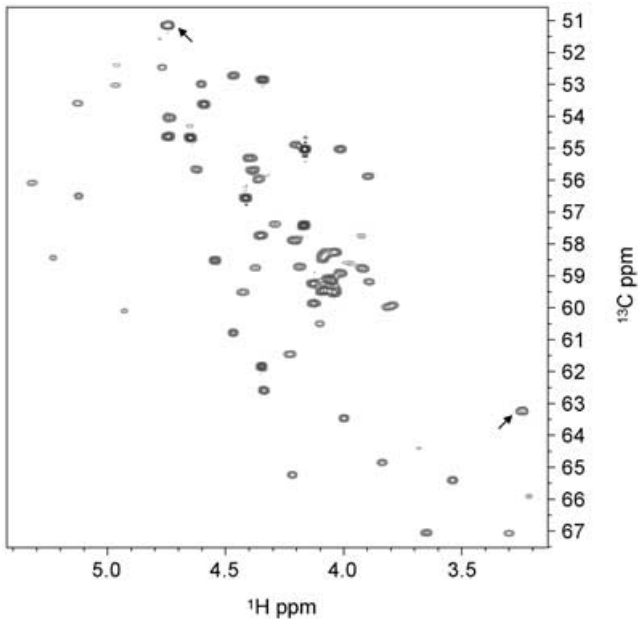

Figure 1. Representative $R_{1\rho}$ spectrum obtained with a relaxation delay of 40 ms. $^{1}H,^{13}C$ correlations are observed for all carbons with an odd number of protons attached, while glycine residues are rejected. Folded peaks of opposite phase are marked with arrows and represent side-chain carbons that are covalently connected to an even number of aliphatic ^{13}C spins. The lowest contour is plotted above the noise level.

$R_{1\rho}$ decay curves

The strong scalar couplings and similar chemical shifts among aliphatic ^{13}C spins, between $^{13}C^{\alpha}$ and $^{13}C'$, and between neighboring $^{13}C^{\alpha}$ spins can cause detrimental magnetization transfer due to Hartmann–Hahn matching throughout the coupled network of ^{13}C spins.[37] Provided that the spin-lock fields are calibrated accurately and that all resonances are assigned, Hartmann–Hahn matching conditions can be identified from Equation (5) to exclude any data points that are subject to significant magnetization transfer. In the present application, in which the spin-lock carrier is positioned in the middle of or downfield from the $^{13}C^{\alpha}$ region, problems are mainly due to Hartmann–Hahn transfer through the one-bond ($^{1}J_{CC} = 55$ Hz) to the $^{13}C'$ spins of the backbone, and three-bond ($^{3}J_{CC} = 5$ Hz) couplings to neighboring $^{13}C^{\alpha}$ spins and $^{13}C'$ in Glu/Gln side chains. The large one-bond coupling constant renders Hartmann–Hahn transfer active even for relatively large differences in resonance frequencies ("mismatching") between the coupled spins. Additional problems can be anticipated for Ser and Thr, since their $^{13}C^{\beta}$ resonates in the same spectral region as $^{13}C^{\alpha}$.

Representative decay curves are shown in Figure 2. The large majority of decays are well represented by monoexponential functions, as exemplified for S81 at nominal spin-lock carrier offsets of 8000 and 4000 Hz (Figure 2A, B), but for a subset of spin-lock parameters (θ, ω_{eff}) some residues have decays that are convoluted with the Hartmann–Hahn transfer function, as exemplified for S81 with the spin-lock carrier on resonance (Figure 2C; see also Equation (5)). Our criterion based on Equation (5) correctly pinpointed all such $R_{1\rho}(\theta, \omega_{eff})$

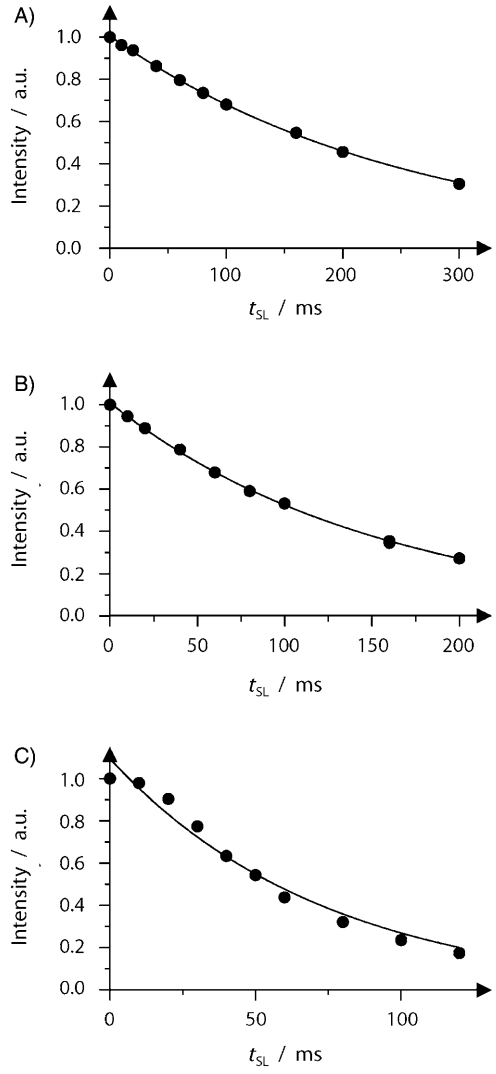

Figure 2. Decay rates for residue S81 at offsets of $\Omega = 7934$ Hz (A), 3974 Hz (B), and -26 Hz (C) at a spin-lock field strength of $\gamma B_1/2\pi = 2572$ Hz. The line represents the best fit to a monoexponential decay. The estimated errors in intensity are approximately the same size as the symbols. Significant effects from Hartmann–Hahn matching are evident in C.

data points (open symbols in Figure 3C, below), which were excluded from the relaxation dispersion data sets prior to fitting exchange parameters. On average, five $R_{1\rho}(\theta, \omega_{eff})$ data points were excluded from the relaxation dispersion curve in the case of Thr and Ser residues, and one data point (in many cases zero) in the case of all other amino acid residues. In agreement with our predictions, there are no signs of multi-exponential decays arising from dipolar cross-relaxation with the $^{13}C'$ spin (cf. Theory and experimental design).

Relaxation dispersion curves

Figure 3 shows representative relaxation dispersion curves, plotted either as $R_{1\rho}$ versus θ (A–D), or R_2 versus $\omega_{eff}/2\pi$ (E–H). Quantitative analyses involving *F* tests were performed to determine whether a given residue was best represented by a four-parameter model including conformational exchange (R_1, $R_{2,0}$, τ_{ex}, φ_{ex}), or a two-parameter model excluding exchange (R_1, $R_{2,0}$); $p < 0.05$ was considered significant. Figure 3B–D and F–H exemplify relaxation dispersion curves for residues with significant exchange, as evidenced by the clearly decaying profiles in panels F–H. For comparison, Figure 3A and E exemplify relaxation dispersion curves for a residue without exchange, which has a flat profile in E. Conformational exchange was identified for 33 residues. The fraction of residues showing exchange (45%) is on par with the numbers obtained from the ^{15}N and ^1H $R_{1\rho}$ experiments.[11,20] The reduced χ^2 values of the fits range between 0.2–8.5, with an average of 1.2; this indicates that the relaxation dispersion curves are well represented by the selected models.

Laboratory-frame relaxation rates

The weighted average values of R_1 and $R_{2,0}$ are $\langle R_1 \rangle = 2.6 \pm 0.3\ s^{-1}$ and $\langle R_{2,0} \rangle = 10 \pm 4\ s^{-1}$, when the average is taken over all residues. On restricting the average to include only residues located in α-helices and the Ca^{2+}-binding loops, the values become $\langle R_1 \rangle = 2.5 \pm 0.1\ s^{-1}$ and $\langle R_{2,0} \rangle = 16 \pm 3\ s^{-1}$. These numbers agree well with the rates expected for a protein with an isotropic rotational diffusion time constant of $\tau_c = 4.2$ ns and an order parameter of $S^2 = 0.8$: $R_1 = 2.6\ s^{-1}$ and $R_{2,0} = 17\ s^{-1}$. The good agreement between the calculated and experimentally determined laboratory-frame relaxation rates further indicates that the $^{13}C^\alpha$ $R_{1\rho}$ method is robust. The relatively large standard deviations are due to variation across the protein in fluctuation amplitudes on the picosecond-to-nanosecond timescale, with the helices and Ca^{2+}-binding loops having significantly lower mobility than the linker loop and N and C termini; these results are perfectly consistent with previous results from ^{15}N laboratory-frame relaxation.[29]

Exchange correlation times, τ_{ex}

Figure 4A shows the optimized exchange correlation times, τ_{ex}, for all residues with significant exchange contributions to R_2. As expected for a global process, τ_{ex} exhibits limited variation across the protein. The weighted-average exchange correlation time is $\langle \tau_{ex} \rangle = 25 \pm 8$ μs, in excellent agreement with the previously determined values of 21 ± 3 and 19 ± 7 μs from ^{15}N and ^1H $R_{1\rho}$ experiments, respectively.[11,20] The apparent site-to-site variability in τ_{ex} is 13 μs, compared with 3 μs for ^{15}N.[11] Global optimization of τ_{ex} against the relaxation dispersion curves of all residues exhibiting exchange yields $\tau_{ex} = 27 \pm 1$ μs.

Populations and chemical-shift differences, φ_{ex}

Figure 4B shows the fitted parameter φ_{ex}, which carries information on the relative populations of the exchanging conformations and the chemical-shift difference between them: $\varphi_{ex}^{1/2} = (p_A p_B)^{1/2} \Delta\omega$. As observed, φ_{ex} ranges between $(0.6–6.0) \times 10^5\ s^{-2}$. Given a global two-state exchange model, the variation in $\varphi_{ex}^{1/2}$ corresponds to the variation in residue-specific chemical-shift differences. As mentioned above, $^{13}C^\alpha$ chemical shifts

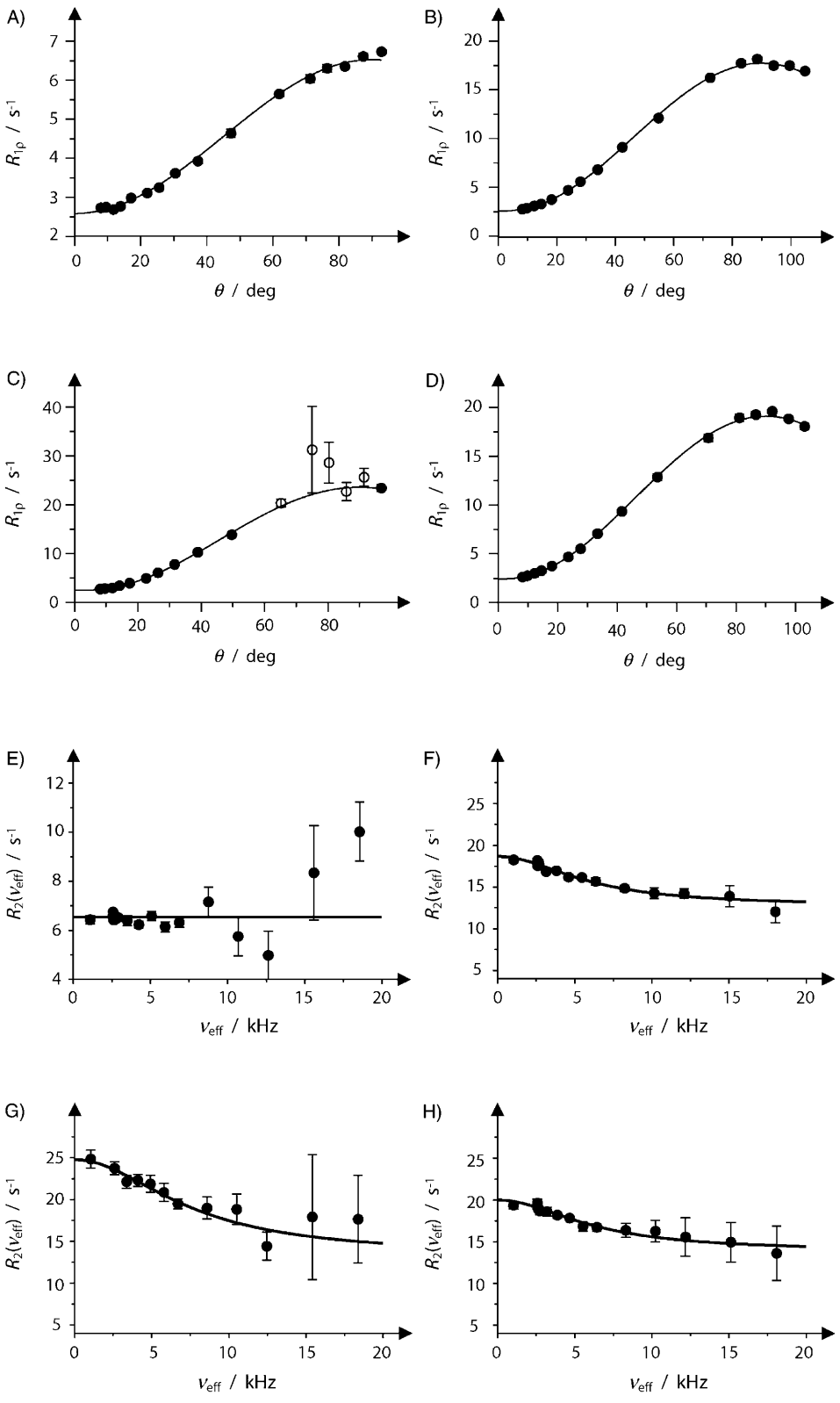

Figure 3. Representative $^{13}C^{\alpha}$ $R_{1\rho}$ relaxation dispersion curves. A)–D) $R_{1\rho}$ plotted as a function of the tilt angle, θ. ●: data recorded with $\omega_1/2\pi = 2572$ Hz and different nominal spin-lock carrier offsets ($\Omega/2\pi$) from the midpoint of the spectrum, covering the range from −0.5 to 20 kHz. ○: data that are subject to Hartmann–Hahn matching conditions, cf. Equation (5). E)–H) R_2 plotted as a function of the effective field strength, $\omega_{eff}/2\pi$. R_2 was calculated from the $R_{1\rho}$ data: $R_2 = R_{1\rho}/\sin^2\theta - R_1/\tan^2\theta$. The full line represents the best-fit model, which comprises four parameters (including conformational exchange) in the case of residues E83 (panels B, F), S101 (C, G), and Q143 (D, H) and two parameters (without exchange) for M76 (A, E). Note that the vertical scale is different in E. For clarity, on-resonance $R_{1\rho}$ values obtained with varying B_1 field strengths were omitted from these plots.

depend strongly on the φ and ψ dihedral angles. All of the twenty different types of amino acid residue show the same dependence on φ and ψ in that the chemical shift decreases upon going from α-helical, through random coil, to β-strand conformation. Previous work on E140Q–Tr2C has indicated that the exchanging populations are nearly equal.[11,20,29,38] Hence, the chemical-shift differences can be obtained as $\Delta\omega = 2\varphi_{ex}^{1/2}$, or $\Delta\delta_{ex} = 2\varphi_{ex}^{1/2}/\gamma_C B_0$ in units of ppm. The weighted average thus obtained for E140Q–Tr2C is $\langle\Delta\delta_{ex}\rangle = 1.3 \pm 0.4$ ppm, with individual shift differences covering the range from 0.6 to 1.9 ppm. Global optimization of τ_{ex} results in residue-specific $\Delta\delta_{ex}$ values that differ by 27%, on average, from those obtained for the residue-specific fits of τ_{ex} (data not shown). These values can be compared to the maximum secondary shifts of approximately +4 ppm for α-helices and −4 ppm for β-sheets in Tr2C. Another point of reference is the 2.2 ppm average rms deviation from the mean for $^{13}C^{\alpha}$ chemical shifts in the BioMagResBank (see above). Clearly, the extracted $\Delta\delta_{ex}$ values are physically reasonable, and their absolute magnitudes suggest that the conformational fluctuations correspond to excursions within a single region of the Ramachandran diagram, that is, there is no evidence of large-scale transitions between either α-helical or β-sheet conformations and random coil. However, the extracted shift differences agree poorly with those expected from the wild-type chemical shifts of the apo and Ca^{2+}-loaded states, $\Delta\delta_{wt}$, which are very small; the rms difference between $\Delta\delta_{ex}$ and $\Delta\delta_{wt}$ is 1.3 ppm, with $\Delta\delta_{ex}$ generally being larger than $\Delta\delta_{wt}$. This observation is in contrast

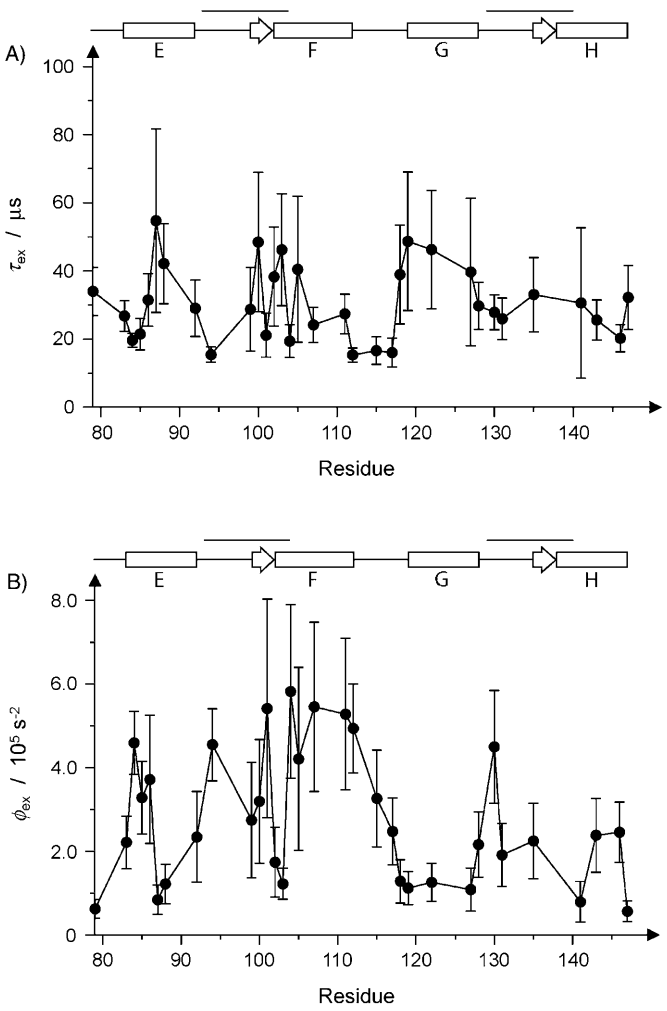

Figure 4. The fitted exchange parameters A) τ_{ex} and B) φ_{ex} plotted against residue number. The secondary-structure elements and calcium-binding loops are indicated above the graph.

with previous results from ^{15}N experiments, for which good agreement was generally obtained between $\Delta\delta_{ex}$ and $\Delta\delta_{wt}$.[11] The variation in $\Delta\delta_{ex}$ across E140Q–Tr2C indicates that certain regions experience significantly larger conformational changes than others (Figure 4B). Notably, a segment of helix E and all of helix F appear to undergo larger changes in chemical shifts than the other helices. ANOVA analyses[39] indicate that $\Delta\delta_{ex}$ varies significantly between helices ($p = 0.0057$). Furthermore, multiple comparison ANOVA by using Tukey's method shows that helix F has significantly larger $\Delta\delta_{ex}$ than the other three helices (at level $\alpha = 0.05$), which are not significantly different from one another. Interestingly, both the ^{15}N $R_{1\rho}$ and ^{15}N,^{1}H multiple-quantum relaxation rates of residues in helix F agree relatively poorly with the model predicting exchange exclusively between wild-type-like conformations.[11,38] However, the discrepancies between $\Delta\delta_{ex}$ and $\Delta\delta_{wt}$ are much more prominent in the ^{13}C data than in the ^{15}N or ^{1}H data. Apparently, the exchange in E140Q–Tr2C involves larger fluctuations in backbone dihedral angles than expected from the simple open–closed model, in which the secondary-structure elements remain essentially intact. The increased chemical-shift differences observed for helix F suggest that it samples partially frayed conformations.

Conclusion

The $^{13}C^{\alpha}$ off-resonance $R_{1\rho}$ experiment presented here significantly extends the timescale of exchange dynamics that can be studied by using ^{13}C, compared to previously described CPMG approaches. By using on-resonance spin-lock field strengths of 2500 Hz, it is possible to sample the dispersion profile beyond the inflection point for exchange correlation times in the order of 70 µs. By including off-resonance $R_{1\rho}$ data, we reliably quantitated conformational exchange with $\tau_{ex} < 30$ µs. This is in contrast to the case for ^{15}N, in which additional laboratory-frame relaxation data are required to determine the exchange parameters' reliably.

The different dependencies of $^{13}C^{\alpha}$, ^{15}N, and ^{1}H chemical shifts on conformational parameters—such as backbone and side-chain dihedral angles, hydrogen bonds, long-range ring-currents, and electrostatic interactions—provide highly complementary information on the structure of the exchanging states. The present results underscore the advantage of using several types of nuclei to probe exchange dynamics in biomolecules.

Experimental Section

Theory and experimental design: The rotating-frame autorelaxation rate is given by:[9,40]

$$R_{1\rho} = R_1 \cos^2\theta + (R_{2,0}+R_{ex})\sin^2\theta \quad (1)$$

Here R_1 is the longitudinal relaxation rate, $R_{2,0}$ and R_{ex} are the exchange-free and exchange contributions to the transverse relaxation rate, respectively, $\theta = \arctan(\omega_1/\Omega)$ is the tilt angle between the static magnetic field and the RF field ω_1, and Ω is the resonance offset from the carrier frequency. For $^{13}C^{\alpha}$, the auto-relaxation rates R_1 and $R_{2,0}$ are dominated by the dipolar interaction with the attached proton, but also depend on the chemical-shift anisotropy as shown by the following expressions:

$$R_1 = (d^2/4)(3J(\omega_C) + 6J(\omega_H+\omega_C) + J(\omega_H-\omega_C)) + c^2J(\omega_C) \quad (2)$$

$$R_{2,0} = (d^2/8)(4J(0) + 3J(\omega_C) + 6J(\omega_H) + 6J(\omega_H+\omega_C) + J(\omega_H-\omega_C)) + (c^2/6)(4J(0) + 3J(\omega_C)) \quad (3)$$

Here $d = \hbar\mu_0\gamma_C\gamma_H\langle r^{-3}\rangle/4\pi$ is the strength of the dipolar interaction between $^{13}C^{\alpha}$ and $^{1}H^{\alpha}$, $c = \gamma_C B_0 \Delta\sigma_C/3^{1/2}$ is the strength of the interaction between the $^{13}C^{\alpha}$ magnetic dipole and the anisotropic local field due to chemical shielding, $J(\omega) = 2/5 \times S^2\tau_c/(1+\omega^2\tau_c^2)$ is the spectral density function, S^2 is the square of the generalized order parameter,[41,42] τ_c is the correlation time of overall rotational diffusion, $\hbar$ is Planck's constant divided by 2π, γ_i is the gyromagnetic ratio of spin i, r is the distance between the $^{1}H^{\alpha}$ and $^{13}C^{\alpha}$ nuclei, B_0 is the static magnetic-field strength, and $\Delta\sigma_C$ is the chemical-shielding anisotropy of $^{13}C^{\alpha}$. In principle, cross-relaxation with the $^{13}C'$ spin renders the $^{13}C^{\alpha}$ rotating-frame relaxation multiexponential. However, calculations indicate that this effect introduces less than 1% error into the extracted $R_{1\rho}$ values, thus indicating that it can safely be neglected.

R_{ex} arises from stochastic modulation of the isotropic chemical shift due to motions slower than overall rotational diffusion. The functional form of R_{ex} depends primarily on the ratio between the rate of exchange, $k_{ex}=1/\tau_{ex}$, and the chemical-shift difference between the exchanging states, $\Delta\omega$.[9,10] For fast conformational exchange ($k_{ex}/\Delta\omega \gg 1$) between two states A and B, R_{ex} is given by:[43,44]

$$R_{ex} = \frac{\varphi_{ex}\tau_{ex}}{1+\omega_1^2\tau_{ex}^2} \quad (4)$$

Here $\varphi_{ex}=p_A p_B \Delta\omega^2$, p_A and p_B are the populations of the substates, and $\omega_{eff}=(\omega_1^2+\Omega^2)^{1/2}$ is the effective field strength of the spin-lock. By performing experiments at different effective fields, it is thus possible to determine the parameters τ_{ex} and φ_{ex}.

The large scalar couplings to C′ and C^β of 55 and 35 Hz, respectively, is a serious concern in the present $R_{1\rho}$ experiments. In contrast to CPMG-type experiments, $R_{1\rho}$ measurements do not suffer from COSY-type transfer to scalar coupled spins.[21,24] However, in the presence of a spin-lock field, homonuclear Hartmann–Hahn matching can be realized for certain tilt angles and effective fields;[37] this complicates the extraction of reliable relaxation rates.[22] The Hartmann–Hahn transfer function between two scalar coupled spins, I and S, is given by:[45]

$$F_{HH} = \frac{1}{1+(\Delta/J_{eff})}\sin^2(Dt_{SL}/2) = A_{HH}\sin^2(Dt_{SL}/2) \quad (5)$$

Here A_{HH} is the amplitude of the transfer function, $D=(\Delta^2+J_{eff}^2)^{1/2}$, $\Delta=\omega_{eff,I}-\omega_{eff,S}$ is the mismatch, $\omega_{eff,i}$ is the effective field strength experienced by spin i, $J_{eff}=J[1+\cos(\theta_I-\theta_S)]/2$ is the effective coupling constant, J is the scalar coupling constant, and t_{SL} is the mixing time. Given the parameters of the present continuous-wave spin-lock experiments (see below), Hartmann–Hahn transfer is highly efficient for certain combinations of tilt angles and effective fields, and it is crucial to exclude these data points from the analysis. We excluded any $R_{1\rho}(\theta, \omega_{eff})$ data points for which $A_{HH} > 0.01$.

Glycine residues cannot be analyzed in the case of non-deuterated samples, since cross correlation between the two dipolar C–H interactions leads to multiexponential decays, and since the present pulse sequence rejects signals from $^{13}C\text{-}H_2$ spin systems. By contrast, it would be straightforward to measure $R_{1\rho}$ for $^{13}C^\alpha$ of Gly residues in partially deuterated samples, because the selected ^{13}C-H-D spin system does not suffer from dipolar cross correlation. By using this approach it is possible, in principle, to measure $R_{1\rho}$ of virtually any CHD or CHD_2 group in a protein, although Hartmann–Hahn matching is expected to pose severe restraints on the values of θ and ω_{eff} that can be used for a given methylene or methyl group. It should also be pointed out that the present $R_{1\rho}$ experiment is useful for probing other methine carbons besides $^{13}C^\alpha$, that is $^{13}C^\beta$ of Ile, Thr, and Val and $^{13}C^\gamma$ of Leu. However, the spin-lock carrier offsets might need to be optimized in each specific case.

One drawback of the $^{13}C^\alpha$ $R_{1\rho}$ experiment, compared to the equivalent ^{15}N experiment,[46] is that transverse relaxation is significantly larger for $^{13}C^\alpha$; this reduces the sensitivity to conformational exchange. However, since CSA-mediated autorelaxation is small for $^{13}C^\alpha$, the experiment can be advantageously run at higher static fields without a significant increase in the exchange-free autorelaxation rate, leading to improved sensitivity towards conformational exchange. The resolution in a ^{15}N HSQC is typically superior to that in the C^α region of a ^{13}C HSQC. However, overlap problems can be overcome by extending the experiment to include the carbonyl resonance frequency in a third dimension. Magnetization transfer to $^{13}C'$ is efficient due to the 55 Hz scalar coupling constant, and the relaxation rate of $^{13}C'$ is modest. Reverse accordion strategies may be employed to alleviate the increase in acquisition time required for three-dimensional experiments.[47] Overlap in the ^1H dimension with the residual solvent resonance is hard to avoid unless extreme care is taken to obtain a proton-free sample. In the present case, we dissolved the sample in 100% D_2O, but used protonated chemicals to adjust the pH.

Sample preparation: Uniformly $^{13}C/^{15}N$-enriched E140Q–Tr2C was obtained by overexpression in *Escherichia coli* MM294 by using ^{13}C-glucose and $^{15}NH_4Cl$ as the sole carbon and nitrogen sources. The NMR sample consisted of $^{13}C/^{15}N$-labeled E140Q–Tr2C (1.0 mM) supplemented with $CaCl_2$ (20 equiv), 2,2-dimethyl-2-silapentane-5-sulfonic acid (DSS; 100 μM) and NaN_3 (200 μM) in 100% D_2O at pH 6.0.Under these conditions, the calcium-saturated state is populated to >98%.[28]

NMR spectroscopy: All experiments were performed on a Varian INOVA spectrometer operating at a ^1H Larmor frequency of 499.86 MHz. The temperature set point was 28.0 °C. The temperature was calibrated by measuring the frequency difference between the DSS and solvent resonances. Heat-compensation pulses were implemented as described to avoid differential heating for different RF field strengths and relaxation delays.[48] In all experiments, 67 and 512 complex points were recorded in evolution periods t_1 and t_2, respectively. The recycle delay was 1 s. $R_{1\rho}$ rate constants were measured by using the pulse sequence shown in Figure 5. The experiment is similar to previously described ^{15}N $R_{1\rho}$ experiments,[1,11,49] but includes constant-time evolution in t_1 to refocus scalar couplings with covalently attached aliphatic carbons.[50] The data were recorded in an interleaved fashion as three-dimensional arrays, where the first and second dimensions correspond to the t_1 and t_2 evolution periods, and the third dimension to the relaxation delay t_{SL}. Adiabatic alignment of the magnetizations with their respective effective fields during the spin-lock relaxation period and subsequent return to the z-axis were achieved by using tan/tanh RF frequency/amplitude ramps;[51,52] this provides satisfactory alignment at high-RF field strengths.[49] On-resonance experiments were performed with the carrier placed at 58.0 ppm and RF field strengths of 1026±19 and 2572±109 Hz. In addition, we recorded off-resonance experiments using a constant RF spin-lock field strength of $\omega_1=2572$ Hz and offsets of $\Omega=-500$, -250, 250, 500, 1000, 2000, 3000, 4000, 5000, 6000, 8000, 10000, 12000, 15000, and 18000 Hz. Spin-lock field strengths were calibrated as described previously.[22] For each effective field, the decay was sampled by using nine or ten data points, with the longest relaxation delay ($t_{SL}=300$ ms) selected so as to sample the decay beyond $1/R_{1\rho}$. Thus, the maximum value of t_{SL} is kept shorter than $1/R_1$.[27]

Data processing and analysis: All data were processed by using nmrPipe.[53] The data were extended by 30 points in t_1 by using linear prediction, apodized in t_1 and t_2 with cosine and Lorentzian-to-Gaussian window functions, respectively, and zero-filled to 512 and 4096 points prior to Fourier transformation. Peak volumes were estimated by summing 3×5 ($t_1\times t_2$) points centered on the peak maximum. Extraction of $R_{1\rho}$ decay rates and exchange parameters was performed with in-house software. Monoexponential functions were fitted to the decays at each tilt angle. The $R_{1\rho}$ dispersion curves were fitted by using both a two-parameter model that included R_1 and $R_{2,0}$, corresponding to Equation (1) with $R_{ex}=0$, and a four-parameter model that included R_1, $R_{2,0}$, τ_{ex}, and φ_{ex}, corresponding to Equations (1) and (4). Individual $R_{1\rho}(\theta, \omega_{eff})$ data points for which Hartmann–Hahn transfer to either C′ or C^β exceeded 1%, as determined from Equation (5), were not included in the

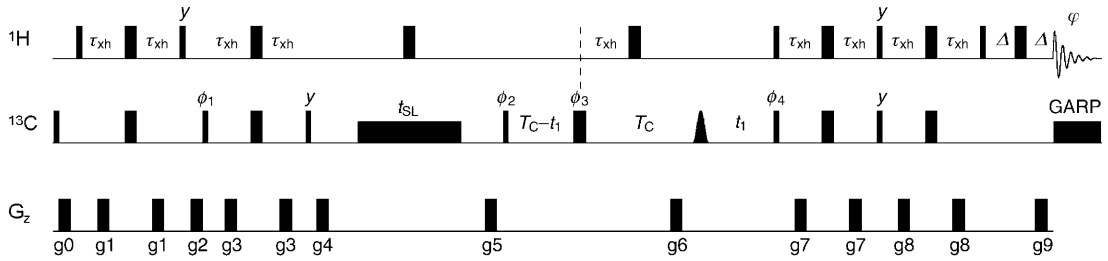

Figure 5. Pulse sequence to measure methine ^{13}C $R_{1\rho}$ relaxation rates. Narrow and broad pulses correspond to flip angles of 90° and 180°, respectively. Proton pulses were centered at 4.74 ppm, and carbon pulses were centered at 58.0 ppm. The carbon carrier was moved to the spin-lock offset after gradient g4 and back before gradient g5. The shaped pulse in the constant time evolution period is used to invert the carbonyl spins and was implemented as a G3 pulse of 514 μs duration centered at 177 ppm.[56] A rectangular inversion pulse was applied on ^{15}N simultaneously with the carbonyl pulse (not shown). A continuous-wave RF field was applied far off resonance on the ^{13}C channel to avoid differential heating for different relaxation delays and field strengths (not shown).[48] Decoupling during acquisition utilized the GARP-1 sequence with a field strength of $\gamma B_1/2\pi = 2350$ Hz.[57] The delays were $\tau_{xh} = 1/(4^1J_{CH})$, $T_C = 13.3$ ms, and $\Delta = 0.6$ ms. The phase cycle was $\varphi_1 = x, -x$; $\varphi_2 = x$; $\varphi_3 = x, x, y, y, -x, -x, -y, -y$; $\varphi_4 = x$; $\phi_{rec} = x, -x, -x, x$. Gradient strengths (lengths) were g0 = 5000 (1.0 ms), g1 = 4000 (0.8), g2 = 13 000 (1.0), g3 = 5000 (0.8), g4 = −17 000 (1.2), g5 = 13 000 (0.8), g6 = 15 000 (1.0), g7 = 4000 (1.0), g8 = 4000 (1.0), g9 = 14 920 G cm^{-1} (0.25). Quadrature detection in t_1 was implemented by inverting the phase φ_1 together with the gradient g9. The phases of φ_4 and ϕ_{rec} were inverted in every other increment to achieve states–TPPI phase cycling.[58]

optimization of the exchange parameters. *F* tests were used to determine the appropriate model; $p < 0.05$ was considered significant.[39] Errors in fitted parameters were estimated by Monte-Carlo simulations[54] or the jack-knife procedure.[55]

Acknowledgements

We thank Eva Thulin for assistance with protein expression and purification. This work was supported by project grants from the Swedish Research Council (VR) and the Swedish Foundation for Strategic Research (SSF), and an instrumentation grant from the Knut and Alice Wallenberg Foundation.

Keywords: biophysics · calmodulin · metalloproteins · molecular dynamics · NMR spectroscopy

[1] M. Akke, R. Brüschweiler, A. G. Palmer, *J. Am. Chem. Soc.* **1993**, *115*, 9832 – 9833.
[2] D. Yang, L. E. Kay, *J. Mol. Biol.* **1996**, *263*, 369 – 382.
[3] A. L. Lee, S. A. Kinnear, A. J. Wand, *Nat. Struct. Biol.* **2000**, *7*, 72 – 77.
[4] E. Z. Eisenmesser, D. A. Bosco, M. Akke, D. Kern, *Science* **2002**, *295*, 1520 – 1523.
[5] M. Wolf-Watz, V. Thai, K. Henzler-Wildman, G. Hadjipavlou, E. Z. Eisenmesser, D. Kern, *Nat. Struct. Mol. Biol.* **2004**, *11*, 945 – 949.
[6] A. Malmendal, J. Evenäs, S. Forsén, M. Akke, *J. Mol. Biol.* **1999**, *293*, 883 – 899.
[7] J. Yan, Y. Liu, S. M. Lukasik, N. A. Speck, J. H. Bushweller, *Nat. Struct. Mol. Biol.* **2004**, *11*, 901 – 906.
[8] M. Akke, *Curr. Opin. Struct. Biol.* **2002**, *12*, 642 – 647.
[9] A. G. Palmer, *Chem. Rev.* **2004**, *104*, 3623 – 3640.
[10] A. G. Palmer, C. D. Kroenke, J. P. Loria, *Methods Enzymol.* **2001**, *339*, 204 – 238.
[11] J. Evenäs, A. Malmendal, M. Akke, *Structure* **2001**, *9*, 185 – 195.
[12] B. F. Volkman, D. Lipson, D. E. Wemmer, D. Kern, *Science* **2001**, *291*, 2429 – 2433.
[13] M. J. Grey, C. Wang, A. G. Palmer, *J. Am. Chem. Soc.* **2003**, *125*, 14 324 – 14 335.
[14] M. A. S. Hass, M. H. Thuesen, H. E. M. Christensen, J. J. Led, *J. Am. Chem. Soc.* **2004**, *126*, 753 – 765.
[15] D. M. Korzhnev, X. Salvatella, M. Vendruscolo, A. A. Di Nardo, A. R. Davidson, C. M. Dobson, L. E. Kay, *Nature* **2004**, *430*, 586 – 590.
[16] D. S. Wishart, D. A. Case, *Methods Enzymol.* **2001**, *338*, 3 – 34.
[17] X. P. Xu, D. A. Case, *Biopolymers* **2002**, *65*, 408 – 423.
[18] R. Ishima, P. T. Wingfield, S. J. Stahl, J. D. Kaufman, D. A. Torchia, *J. Am. Chem. Soc.* **1998**, *120*, 10 534 – 10 542.
[19] F. A. A. Mulder, A. Mittermaier, B. Hon, F. W. Dahlquist, L. E. Kay, *Nat. Struct. Biol.* **2001**, *8*, 932 – 935.
[20] P. Lundström, M. Akke, *J. Biomol. NMR* **2005**, in press.
[21] R. Ishima, D. A. Torchia, *J. Biomol. NMR* **2003**, *25*, 243 – 248.
[22] F. A. A. Mulder, M. Akke, *Magn. Reson. Chem.* **2003**, *41*, 853 – 865.
[23] R. Ishima, J. Baber, J. M. Louis, D. A. Torchia, *J. Biomol. NMR* **2004**, *29*, 187 – 198.
[24] F. A. A. Mulder, B. Hon, A. Mittermaier, F. W. Dahlquist, L. E. Kay, *J. Am. Chem. Soc.* **2002**, *124*, 1443 – 1451.
[25] H. Le, E. Oldfield, *J. Biomol. NMR* **1994**, *4*, 341 – 348.
[26] R. B. Hill, C. Bracken, W. F. DeGrado, A. G. Palmer, *J. Am. Chem. Soc.* **2000**, *122*, 11 610 – 11 619.
[27] T. Yamazaki, R. Muhandiram, L. E. Kay, *J. Am. Chem. Soc.* **1994**, *116*, 8266 – 8278.
[28] J. Evenäs, E. Thulin, A. Malmendal, S. Forsén, G. Carlström, *Biochemistry* **1997**, *36*, 3448 – 3457.
[29] J. Evenäs, S. Forsén, A. Malmendal, M. Akke, *J. Mol. Biol.* **1999**, *289*, 603 – 617.
[30] R. Chattopadhyaya, W. E. Meador, A. R. Means, F. A. Quiocho, *J. Mol. Biol.* **1992**, *228*, 1177 – 1192.
[31] B. E. Finn, J. Evenäs, T. Drakenberg, J. P. Waltho, E. Thulin, S. Forsén, *Nat. Struct. Biol.* **1995**, *2*, 777 – 783.
[32] H. Kuboniwa, N. Tjandra, S. Grzesiek, H. Ren, C. B. Klee, A. Bax, *Nat. Struct. Biol.* **1995**, *2*, 768 – 776.
[33] M. Zhang, T. Tanaka, M. Ikura, *Nat. Struct. Biol.* **1995**, *2*, 758 – 767.
[34] H. J. Vogel, *Biochem. Cell Biol.* **1994**, *72*, 357 – 376.
[35] A. Crivici, M. Ikura, *Annu. Rev. Biophys. Biomol. Struct.* **1995**, *24*, 85 – 116.
[36] J. Schleucher, M. Sattler, C. Griesinger, *Angew. Chem.* **1993**, *105*, 1518 – 1521; *Angew. Chem. Int. Ed. Engl.* **1993**, *32*, 1489 – 1491.
[37] S. R. Hartmann, E. L. Hahn, *Phys. Rev.* **1962**, *128*, 2042 – 2053.
[38] P. Lundström, M. Akke, *J. Am. Chem. Soc.* **2004**, *126*, 928 – 935.
[39] J. L. Devore, *Probability and Statistics for Engineering and the Sciences*, Brooks/Cole, Monterey, **1999**.
[40] J. Cavanagh, W. J. Fairbrother, A. G. Palmer, N. J. Skelton, *Protein NMR Spectroscopy: Principles and Practice*, Academic Press, San Diego, **1995**.
[41] B. Halle, H. Wennerström, *J. Chem. Phys.* **1981**, *75*, 1928 – 1943.
[42] G. Lipari, A. Szabo, *J. Am. Chem. Soc.* **1982**, *104*, 4546 – 4559.
[43] D. G. Davis, M. E. Perlman, R. E. London, *J. Magn. Reson.* **1994**, *B104*, 266 – 275.
[44] H. Desvaux, P. Berthault, N. Birlirakis, M. Goldman, *J. Magn. Reson.* **1994**, *A108*, 219 – 229.
[45] F. J. M. van de Ven, *Multidimensional NMR in Liquids. Basic Principles and Experimental Methods*, Wiley, New York, **1995**.
[46] M. Akke, A. G. Palmer, *J. Am. Chem. Soc.* **1996**, *118*, 911 – 912.

[47] P. A. Carr, D. A. Fearing, A. G. Palmer, *J. Magn. Reson.* **1998**, *132*, 25 – 33.
[48] A. C. Wang, A. Bax, *J. Biomol. NMR* **1993**, *3*, 715 – 720.
[49] F. A. A. Mulder, R. A. de Graaf, R. Kaptein, R. Boelens, *J. Magn. Reson.* **1998**, *131*, 351 – 357.
[50] G. W. Vuister, A. Bax, *J. Magn. Reson.* **1992**, *98*, 428 – 435.
[51] K. Ugurbil, M. Garwood, A. R. Rath, *J. Magn. Reson.* **1988**, *80*, 448 – 469.
[52] M. Garwood, Y. Ke, *J. Magn. Reson.* **1991**, *94*, 511 – 525.
[53] F. Delaglio, S. Grzesiek, G. W. Vuister, G. Zhu, J. Pfeifer, A. Bax, *J. Biomol. NMR* **1995**, *6*, 277 – 293.
[54] W. H. Press, B. P. Flannery, S. A. Teukolsky, W. T. Vetterling, *Numerical Recipes in C. The Art of Scientific Computing*, Cambridge University Press, Cambridge, **1988**.
[55] F. Mosteller, J. W. Tukey, *Data Analysis and Regression. A Second Course in Statistics*, Addison–Wesley, Reading, MA, **1977**.
[56] L. Emsley, G. Bodenhausen, *Chem. Phys. Lett.* **1990**, *165*, 469 – 476.
[57] A. J. Shaka, P. B. Barker, R. Freeman, *J. Magn. Reson.* **1985**, *64*, 547 – 552.
[58] D. Marion, M. Ikura, R. Tschudin, A. Bax, *J. Magn. Reson.* **1989**, *85*, 393 – 399.

Received: March 1, 2005
Published online on July 19, 2005

